

In vivo evaluation of a novel nanocomposite porous 3D scaffold in a rabbit model: histological analysis

Saffanah Khuder
Mahmood^{1,2}
Intan-Shameha Abdul Razak¹
Mustafa Saddam Ghaji^{1,3}
Loqman Mohamed Yusof⁴
Zaid Khudhur Mahmood⁵
Mohd Adha Bin P Rameli⁶
Zuki Abu Bakar Zakaria^{1,6}

¹Department of Veterinary Preclinical Science, Faculty of Veterinary Medicine, Universiti Putra Malaysia (UPM), Serdang, Malaysia; ²Department of Veterinary Anatomy, Faculty of Veterinary Medicine, University of Mosul, Mosul, Iraq; ³Department of Anatomy and Histology, Faculty of Veterinary Medicine, University of Basrah, Basrah, Iraq; ⁴Department of Companion Animal Medicine and Surgery, Faculty of Veterinary Medicine, ⁵Department of Veterinary Clinical Studies, Faculty of Veterinary Medicine, ⁶Laboratory of Molecular Biomedicine, Institute of Biosciences, Universiti Putra Malaysia (UPM), Serdang, Malaysia

Correspondence: Saffanah Khuder Mahmood; Zuki Abu Bakar Zakaria
Department of Veterinary Preclinical Science, Faculty of Veterinary Medicine, Universiti Putra Malaysia (UPM), Serdang, Malaysia
Tel +60 3 89 47 2102
Fax +60 3 89 47 2218
Email saffanh.jeber@gmail.com;
zuki@upm.edu.my

Abstract: The healing of load-bearing segmental defects in long bones is a challenge due to the complex nature of the weight that affects the bone part and due to bending, shearing, axial, and torsional forces. An innovative porous 3D scaffolds implant of CaCO₃ aragonite nanocomposite derived from cockle shell was advanced for substitute bone solely for load-bearing cases. The biomechanical characteristics of such materials were designed to withstand cortical bone strength. In promoting bone growth to the implant material, an ideal surface permeability was formed by means of freeze drying and by adding copolymers to the materials. The properties of coating and copolymers supplement were also assessed for bone-implant connection resolutions. To examine the properties of the material in advanced biological system, an experimental trial in an animal model was carried out. Critical sized defect of bone was created in rabbit's radial bone to assess the material for a load-bearing application with a short and extended period assessment with histological evaluation of the incorporated implanted material to the bone of the host. Trials in animal models proved that the material has the capability of enduring load-bearing conditions for long-term use devoid of breaking or generating stress that affects the host bone. Histological examination further confirmed the improved integration of the implanted materials to the host bone with profound bone development into and also above the implanted scaffold, which was attained with negligible reaction of the tissues to a foreign implanted material.

Keywords: bionanocomposite, coated scaffolds, bone replacement, segmental bone defect, histology

Introduction

Repairing bone defects has been studied experimentally since Pharaoh's era. Skull defects post-trepanation were substituted with gold or ivory patches. Regardless of medical progress, even today, large bone defects in load-bearing zones are still considered to be problematic in the medical world. Currently, lost bone is habitually substituted with great bone allograft transplants that have been collected from donors. Otherwise, metallic implants were used. The allograft and metallic implants have weaknesses that interfere with the short and extended term results.¹⁻³

Allografts of large structure have biological merits for example natural bone mineral (hydroxylapatite [HA]) and proteins (eg, bone morphogenetic proteins and collagen fibers) that help transplanted bone integration. Nonetheless, the process of integration is time consuming and frequently imperfect, which leads to undesired resorption or rejection reactions, as well as the possibility to transport infectious agents to the host.^{4,5} On the other hand, metallic implants have the capacity to withstand the load applied onto it. However, their inflexibility could result in the deterioration of

host bone, thereby slackening the implantation over time.^{2,6} Different approaches have been tested to improve the adhesion of metallic implants especially in joint replacements. Coarse superficial topography and diverse coating approaches have enhanced the achievement level of joint prosthetic devices. However, the difficulties in sustaining good bonding and integration to the bone of the host still impose an obstacle.^{1,7,8}

Engineered bone tissue constructs ought to have two major roles when implanted *in vivo*: 1) they offer structural sustenance to neo tissues and 2) promote osteoinduction; these simple properties stimulate cell migration, differentiation, and osteogenesis that result in the formation of new bone.⁹

In the recent years, biomaterial composites have turned out to be a viable substitute of metallic implants. These biomaterials offer many possibilities for vascular grafting and stents, fracture fixations, tendons attachments, and replacement of small bone defects. Composite materials are of interest mainly because of their reduced weight, radiolucency, and/or their lower stiffness which is closer to bone compared to metals.¹⁰ Equally, polymer composites of those biomaterials neither cause interference nor did need any safety measures as that of metal implants, once they are exposed to modern diagnostic tools such as CT or MRI.^{11,12}

In this study, we utilized a composite scaffold that is fabricated from cockle shell-derived CaCO₃ aragonite nanoparticles (CAN), gelatin, dextran, and dextrin as a basis for tissue engineering. This scaffold is now being utilized in a number of tissue engineering applications. Gelatin has attracted attention over the past few years owing to its outstanding biocompatibility, degradation into physiological end products, and appropriate interaction with cells and other macromolecules.^{13–18} Practically, cockle shell-permeable forms are used as bone scaffolds to ascertain an upgraded bone ingrowth and osseointegration, although, fragility and low strength narrow their widespread applications in hard tissue implantations. To be utilized efficiently in weight-bearing parts, the mechanical properties of the cockle shell porous scaffold body have to be enhanced.^{19,20} In the setting of bone tissue engineering, it is also significant to take into consideration that there are different literature views on the association between glutaraldehyde (GTA) crosslinking and mineralization. In some *in vivo* studies, GTA crosslinking revealed to induce calcification.^{21–24} Furthermore, the pore arrangement of the scaffold requires to be defined in relations to penetrability and pore size.^{25–27} In order to attain the desired requirements, coating of the porous scaffold was suggested. The fragility of the porous scaffold is likely to be overcome by coating it with polymer layer.²⁸

Various methods are employed to study the tissue reactions *in vivo* post-implantation. Macroscopic examination of implanted sites allows qualitative measurements of the scaffolds biological reactions.^{29–31}

The biomechanical properties of the implants were accustomed to minimize friction pressure between implants and bones and the superficial characteristics were enhanced to encourage bone growth onto the implant material with a coating technique. The new implants were tried for biocompatibility and safety.

The aim of this study was to evaluate the actual tissue biocompatibility of smart scaffolds fabricated (unpublished data) with and without coated framework as a bone substitute for segment defect repair in weight-bearing settings as well as its potentials in producing an appropriate response in regards to promoting new bone tissue formations within the time frame of study.

Materials and methods

A total of 16 adult male New Zealand White rabbits, aged 8–11 months, weighing 2–4 kg were used in this study. They were divided into 4 groups, each group with 4 animals, and kept for 8 weeks and labeled as group A, B, C and D. Group A rabbits had a part of their radial bone (2 cm) (mid shaft) removed by a bone cutter and the critical size defect (CSD) was left empty without implantation as a control. Group B rabbits were implanted with non-seeded scaffolds (scaffold 5211). Group C rabbits were implanted with non-seeded scaffolds (scaffold 5211 soaked in crosslinked GTA and coated with alginate; 5211_{GTA+Alginate}). Group D rabbits were implanted with non-seeded scaffolds (scaffold 5211 coated with polylactic acid (PLA); 5211_{PLA}) prepared by freeze-drying method. The study protocol was approved by the Animal Care and Use Committee, Faculty of Veterinary Medicine, University Putra Malaysia (UPM; AUP-R015/2015). The rabbits were kept in the Animals Housing Facility, Faculty of Veterinary Medicine, UPM. They were housed and maintained at constant temperature and provided with commercial feed rabbit chow *ad libitum* and water. The handling of the animals was in adherence with the IACUC guidelines. An overnight (12 hours) food and water deprivation period preceded the surgery. The animals were anesthetized using ketamine hydrochloride 35 mg/kg body weight (BW) intramuscularly (I/M) and xylazine hydrochloride 3–5 mg/kg BW I/M; anesthetic maintenance was carried out using halothane and O₂. Post-operative pain was treated with regular analgesics that comprised tramadol hydrochloride 5 mg/kg BW I/M and antibiotic that comprised baytril 5%

w/v 1 mL/10 kg BW subcutaneously. The scaffolds prepared according to Mahmood et al³² by freeze-drying method were used in this experiment. For in vivo post-implantation evaluation, scaffolds 5211, 5211_{GTA+Alginate}, and 5211_{PLA} were used. Scaffolds were selected based on porosity, mechanical strength, Young's modulus, and degradation rate. The novel cockle shell-derived CaCO₃ aragonite nanocomposite scaffolds were cut into cylindrical shape corresponding to the radial bone shape with a diameter of 4 mm and a length of 20 mm. The size of the scaffolds was approximated to the size of radial bone defect. All the surgeries were performed under aseptic conditions in small animal surgery room located within the facilities of the Veterinary Hospital of UPM. A 20 mm CSD was created manually on the left radial bone using a bone cutter. The defect was examined immediately after the removal of the bone chip, while the right limb was left without defect to serve as a negative control for comparative purposes. The scaffolds were inserted into the defect area by a gentle press-fit until it was completely fixed into the defect without the help of a bone plate (Figure 1). The rabbits were euthanized on day 60 post-implantation by giving an overdose of sodium pentobarbital (dolethal 1 mg/kg intravenously; 1 mL =182 mg pentobarbital). Bone samples were then collected for histological analyses.

Following euthanasia at week 8 post-implantation, the radial bones of both limbs of the animals were harvested. The bones were cleaned by removing the surrounding soft tissues, and the scaffold implanted sites were grossly examined prior to being viewed under Nikon SMZ 1500/Japan

stereomicroscope to illustrate any changes in bone formation in different stages during this short period of bone being, and through the complete healing when compared with normal radial bone. The bone specimens were then placed into 10% buffered formalin for histological examination.

For light microscopic examination, the bone specimens were fixed in 10% neutral buffered formalin following gross examination for 7 days at room temperature. Following initial fixation, the bones were further cleaned and washed under running tap water for 30 minutes to 1 hour for large specimens prior to decalcification. The bone specimens were then immersed in 8% formic acid solution and 8% HCl for 7 days. After decalcification, bone processing (dehydration with an increasing concentration of alcohol, clearing with xylene, and then impregnation [embedding] in paraffin wax) was performed automatically using a machine (Leica Microsystem, Wetzlar, Germany). Immediately after embedding, the samples were blocked with paraffin wax and then sectioned using standard histological techniques; exactly 5 µm thick samples were prepared from the center and margin of each sample using rotary microtome (Leica 2045). Cross-section and longitudinal section of bone were prepared.³³ The samples were stained with hematoxylin and eosin (H&E) for general histological observation; Masson's trichrome staining was used to detect collagen fiber and to observe new bone formation.³⁴ The slides were then immersed in xylene and mounted with cover slip using DPX mounting medium.^{19,20,35} In the histological specimens, inflammatory reactions, resorption of host bone, new bone

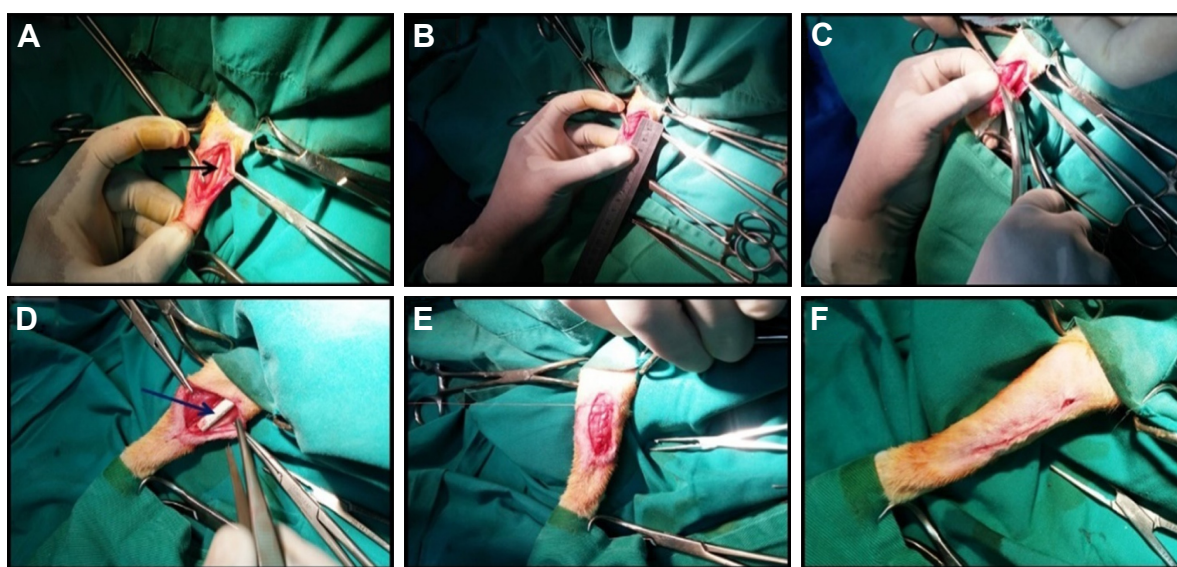


Figure 1 (A–F) Photographs of the surgical procedure of creating a defect in radial bone (black arrow) and scaffold implantation into the defect area in a rabbit model. **Note:** Note that the defect is well fixed with sterilized 3D scaffolds (blue arrow).

formation, and maturation with bone incorporation around the implant were assessed. The slides were examined under a light microscope (Motic BA410; NY Microscope Co., Hicksville, NY, USA) equipped with a camera (Moticam Pro, 285A; NY Microscope Co.). This microscope along with software (Plus 2.0) were used to adjust the images before they were used to examine the bone and show the two forms of mineralized bone: woven (immature) and lamellar (mature) through comparison with the control group and the normal skeleton bone tissue formation.

Results

The results revealed that all the rabbits survived from surgery intervention, and no sign of inflammation or adverse tissue reaction was observed around the implants. Gross examination showed that the radial bone defects in all groups implanted with non-seeded scaffolds showed different levels of healing. Comparatively, the empty defect that was not implanted with scaffolds (group A [control]), the nonunion was observed in the rabbits.

Histological examination of the radial bone defect implanted with scaffolds in groups B, C, and D at day 60 after implantation revealed the formation of new bone replacing the scaffolds. Complete bone healing occurred in defects implanted with 5211_{GTA+Alginate} scaffold at 8 weeks after implantation. Endochondral ossification pattern was observed in this study (Figure 2A and B). Masson's trichrome staining and H&E staining showed normal bone morphology in all implants, which was observed in the restored defects at 8 weeks post-implantation.

Histological examination showed that in control group (group A), the defect bone edge was circular, with only

minimal formation of new bone and cartilage end (Figure 3A and B).

In groups B, C, and D, in which the defects were implanted with scaffolds, histological sections revealed the presence of mature bone and osteoblastic activity. The innermost part of the implant was occupied by bone marrow surrounded by mature bone. Many of the new bone tissues formed were mature and contained plentiful osteocytes. The bone formation showed a centripetal pattern, and the new bone appeared as a replacement of the implant matrix (Figure 4A and B).

In groups B, C, and D, formation of new bone was commonly observed between the implant and the radial bone, and above and below the defect edge and along the implanted scaffolds. Abundant osteoblasts, osteocytes and bone marrow cells were seen in a mature part of implantation at 8 weeks post-implantation (Figure 5A–D).

Only scattered lymphocytes were observed, but no neutrophilic leucocytes were present, as none of the implanted scaffolds was infected. In implanted groups, some giant cells or macrophages were observed. The giant and macrophage cells mostly exist in parts with tissue ingrowth. The cells interact with the matrix, signifying their role in the resorption process (Figure 6A–C). Many new blood vessels (neovascular) of different sizes were noted in the area of new bone formation (Figure 7).

Cartilages were also detected in the upper part of the implant site in group C at 8 weeks. Near the areas of abundant bone formation, the amount of connective tissue was marginal (Figure 8A–D).

In addition, osteoblasts or “lining cells” without an osteoid layer were seen correspondingly with bone formation. The growth of mature bone and medullary cavity occupied

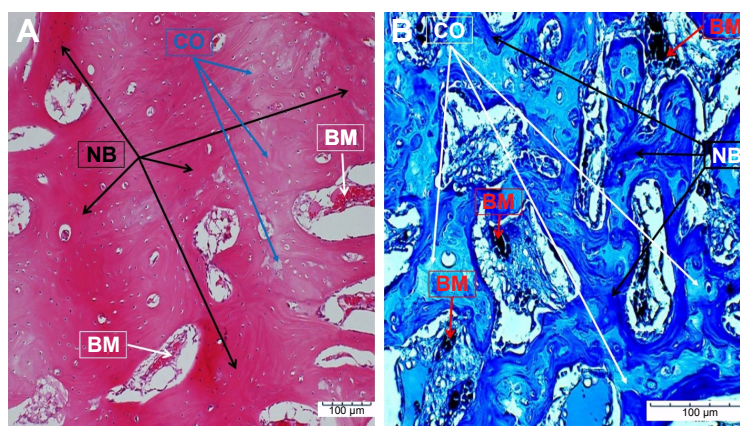


Figure 2 (A, B) Micrographs of the decalcified mature bone of group C at 8 weeks of post-implantation showing new bone formation (NB) and bone marrow (BM).

Notes: The endochondral ossification pattern was observed in this study (CO). Longitudinal section: (A) H&E, ×100 and (B) Masson's trichrome staining, ×200. Group C rabbits were implanted with non-seeded scaffolds (scaffold 5211 soaked in crosslinked GTA and coated with alginate; 5211_{GTA + Alginate}).

Abbreviation: H&E, hematoxylin and eosin.

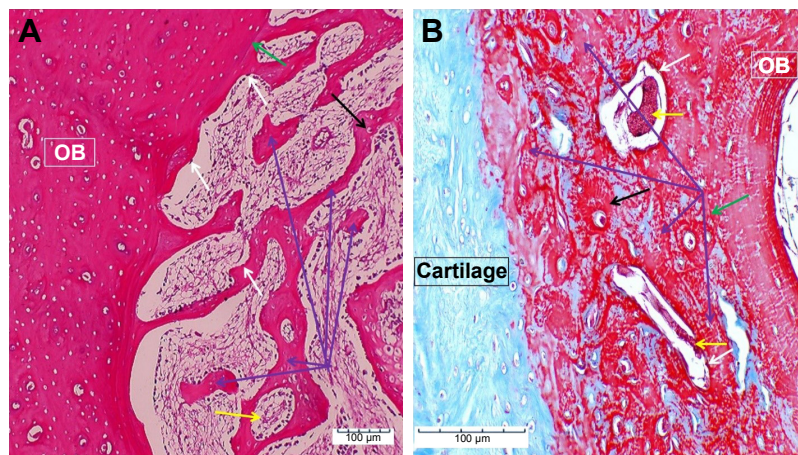


Figure 3 (A, B) Micrographs of the decalcified mature bone of group A (control group) at 8 weeks of post-critical size defect showing the new bone formation (black arrows) and bone marrow (yellow arrows).

Notes: Note the presence of active osteoblast (white arrows), minimal formation of new bone (blue arrows), and the circular defect bone edge (green arrows). Cross section: (A) H&E, $\times 100$ and (B) Masson's trichrome staining, $\times 200$. Group A rabbits had a part of their radial bone (2 cm) (mid shaft) removed by a bone cutter and the critical size defect (CSD) was left empty without implantation as a control.

Abbreviations: H&E, hematoxylin and eosin; OB, original bone.

with bone marrow were also witnessed in newly formed bone. Masson's trichrome staining and H&E staining also showed the presence of mature bone at 8 weeks post-implantation essentially composed of cylindrical unit known as osteons or haversian system. This system consists of concentric lamellae of bone matrix surrounding a central canal, which contains the vascular and nerve supply of the osteon in the mature bone. The canaliculi containing the processes of osteocytes were visible with respect to the canal (Figure 9A–D).

Discussion

This study was conducted due to the clinical need for relevant substitutes of allografts to replace the large section and

weight-bearing bone defects. The disadvantages of using allografts are well acknowledged and these include extended period impediments of metal prostheses used for limb saving surgeries and in addition, the metal implantation and allografts are not integrated to host bone tissue.^{2,3,7,36–38}

In this study, new nanocomposite scaffolds were developed for the purpose of bone replacement. The surface of the scaffold was porous which was created by freeze-drying method and copolymer coating techniques. This was done in an effort to incorporate bone and mechanical linking. The properties of these scaffolds were engineered while considering the weaying consequence of the porosity. The scaffolds structure was biomechanically tried to meet up

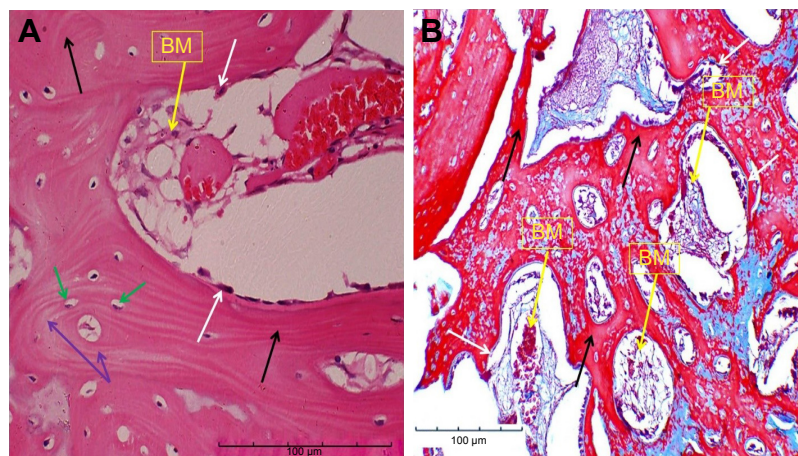


Figure 4 (A, B) Micrographs of the decalcified mature bone of group D at 8 weeks of post-implantation showing new bone formation (black arrows) and bone marrow (BM).

Notes: Note the presence of active osteoblasts (white arrows), plentiful osteocytes (green arrows), and centripetal pattern (purple arrows). Longitudinal section: (A) H&E, $\times 400$ and (B) Masson's trichrome staining, $\times 200$. Group D rabbits were implanted with non-seeded scaffolds (scaffold 5211 coated with PLA; 5211_{PLA}) prepared by freeze-drying method.

Abbreviation: H&E, hematoxylin and eosin.

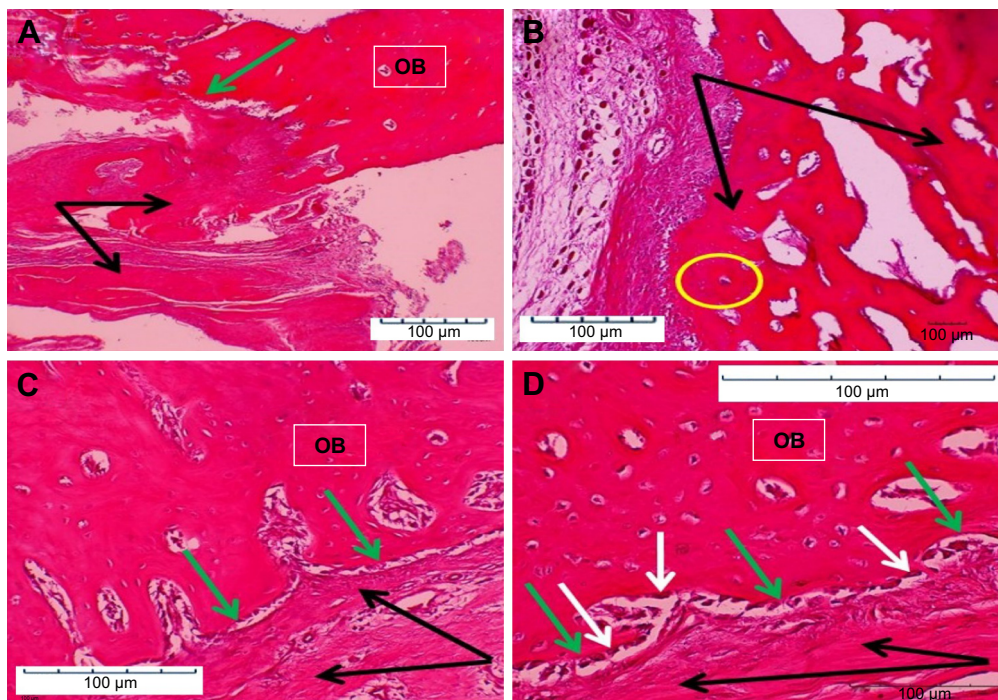


Figure 5 (A–D) Micrographs of the decalcified mature bone of group C at 8 weeks of post-implantation showing the line between the original bone and the developed bone (green arrows) and the new bone formation (black arrows).
Notes: Note the presence of active osteoblasts (white arrows) and the haversian canal containing blood vessels and connective tissues (yellow circle). Longitudinal section: H&E – (A) $\times 40$, (B) $\times 100$, (C), $\times 200$, (D) $\times 400$. Group C rabbits were implanted with non-seeded scaffolds (scaffold 5211 soaked in crosslinked GTA and coated with alginate; 5211_{GTA + Alginate}).
Abbreviation: H&E, hematoxylin and eosin.

with the properties of the bone. This work examined the biological reactions to the new nanocomposite scaffolds in in vitro (unpublished data) and in vivo environment (unpublished data).

The current study gives an insight on the actual tissue response toward the developed nanocomposite scaffolds when used as a bone implant material. The primary aim of the

in vivo studies was to evaluate tissue biocompatibility as an extended observation in order to support excellent cell biocompatibility, which was proven by previous in vitro evaluation (unpublished data). Alternatively, the ability of the developed nanocomposite scaffolds to promote bone defect healing and the quality of its healing is a crucial factor taken into consideration in this part of the study. This is mainly due to the fact

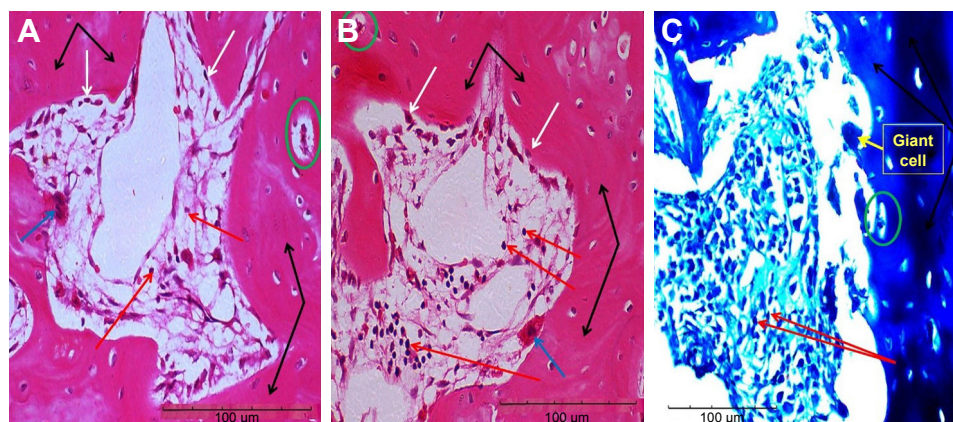


Figure 6 (A–C) Micrographs of the decalcified mature bone of group C at 8 weeks post-implantation showing new bone formation (black arrows) and bone marrow (red arrows).
Notes: Note the presence of osteon (green circles), active osteoblast (white arrows), and giant cell (yellow and blue arrows). (A, B) H&E and (C) Masson's trichrome staining, $\times 400$. Group C rabbits were implanted with non-seeded scaffolds (scaffold 5211 soaked in crosslinked GTA and coated with alginate; 5211_{GTA + Alginate}).
Abbreviation: H&E, hematoxylin and eosin.



Figure 7 Micrograph of the decalcified mature bone of group B at 8 weeks of post-implantation showing the haversian canal containing blood vessel and connective tissue (yellow arrows).

Notes: Longitudinal section: H&E, $\times 400$. Group B rabbits were implanted with non-seeded scaffolds (scaffold 521 I).

Abbreviation: H&E, hematoxylin and eosin.

that the scaffolds developed and used in the current study are neither incorporated with any form of growth promoting-factor nor seeded with stem cells or bone marrow aspirates as traditionally done with the newer generation of bone scaffolds.

During the experimental period, all animals remained in good health and showed no signs of wound or surgical complications. Gross examinations conducted visually and via stereomicroscope, however, showed a healthy appearance of the radial bone and proper healing without signs of degeneration, osteolysis, or inflammation. The absence of inflammation or signs of unwanted tissue reactions allows the classification of a developed scaffolds nanocomposite material as a suitable bone substitute material that facilitates cell attachment and growth.³⁹

Assessment of bone formation was done by histological sectioning qualitatively at the deformed site implanted with nanocomposite scaffolds. Histological findings showed total formation of new bone at the defect site that implanted using the non-seeded implant scaffolds (5211_{GTA+Alginate}) in group C. Nevertheless, in group A

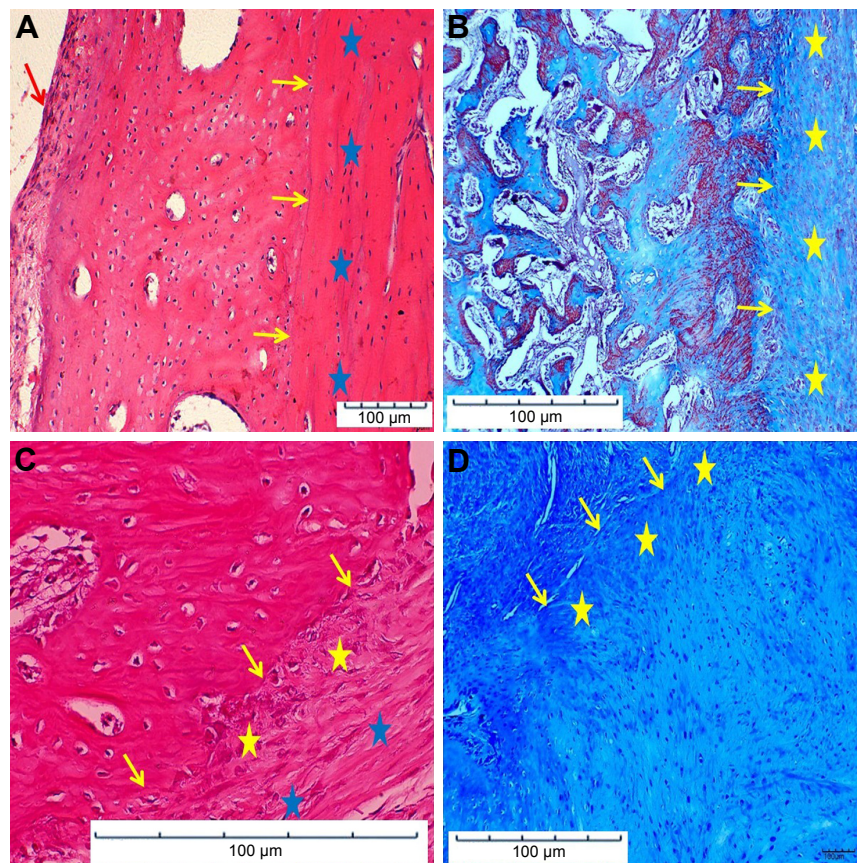


Figure 8 (A–D) Micrographs of the decalcified mature bone of group C at 8 weeks post-implantation showing connective tissues (yellow stars) with intense collagen staining (B–D) and complete bone formation with the presence of periosteum (red arrow) (A).

Notes: The margin is obvious between the new bone (yellow arrows) and the collagen fiber (blue stars) (A, C). Longitudinal section: (A, C) H&E, $\times 40$ and $\times 400$; (B, D) Masson's trichrome staining, $\times 100$. Group C rabbits were implanted with non-seeded scaffolds (scaffold 521 I soaked in crosslinked GTA and coated with alginate; 5211_{GTA+Alginate}).

Abbreviation: H&E, hematoxylin and eosin.

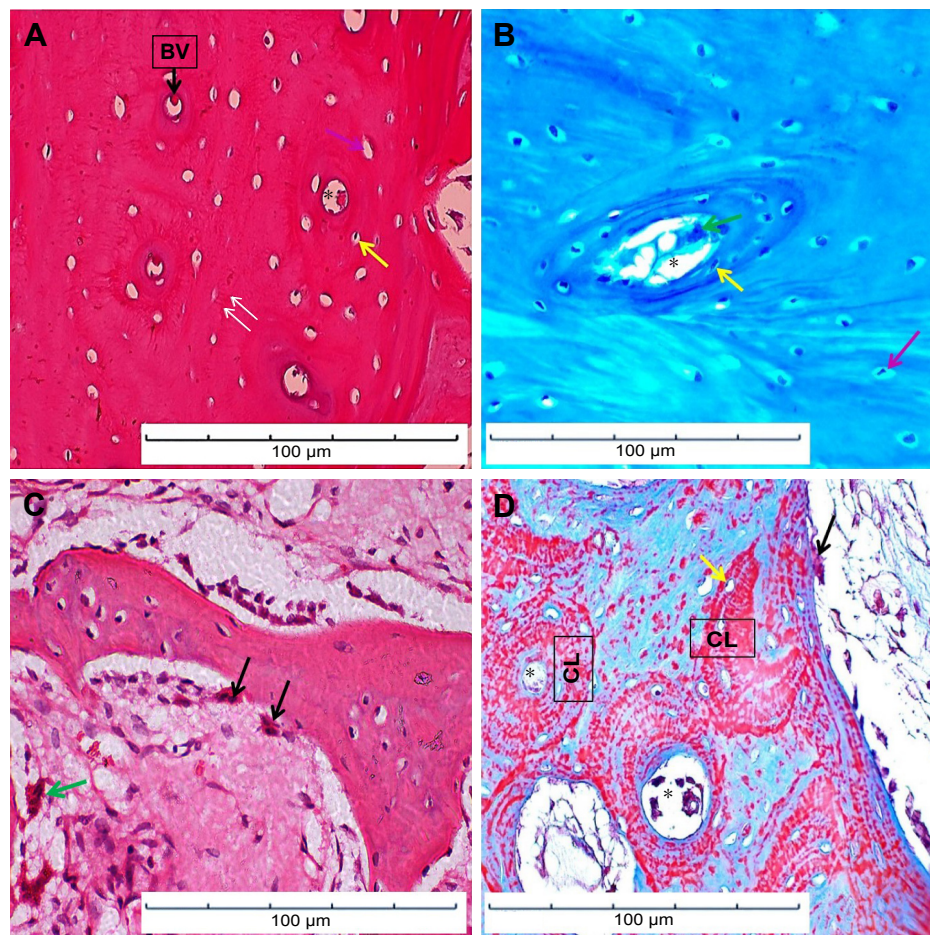


Figure 9 Micrographs of the decalcified bone of implanted group C (A–C) and group D (D) at 8 weeks post-implantation showing the presence of giant cells and macrophages in areas with tissue ingrowth.

Notes: Note remodeling process (black arrows), endosteum (green arrows) in a haversian canal (*), inner circumferential lamellae (CL), and nuclei (yellow arrows) of osteocytes, lacunae (purple arrow) with thin radiating canaliculi (white arrows), and blood vessels (BV). Also note shrunk osteocyte nuclei in lacunae. Longitudinal section: (A, C) H&E and (B, D) Masson's trichrome staining, $\times 400$. Group C rabbits were implanted with non-seeded scaffolds (scaffold 5211 soaked in crosslinked GTA and coated with alginate; 5211_{GTA+Alginate}). Group D rabbits were implanted with non-seeded scaffolds (scaffold 5211 coated with PLA; 5211_{PLA}) prepared by freeze-drying method.

Abbreviation: H&E, hematoxylin and eosin.

(control group) and group B, the formation of the bone was not comprehensive, a blank defect space at the mid of the deformed site was observed, and no osteogenesis was noted at the midpoint of the implant. While in group D, the formation of bone was not completed and a defect space of the deformed site toward the distal part was observed. In this research, in those animals that were implanted with non-seeded scaffolds (group C), the formation of new bone was observed at the middle of the implant. Non-seeded scaffold 5211_{GTA+Alginate} (group C) was totally resorbed at week 8 after implantations and there were whole formation of new bone substituting the implantation, mineralization of new bone and restoration which was confirmed through osteoclast cells appearance. From our observation, we therefore deduce that rapid formation of new bone in animals

implanted with non-seeded scaffolds was due to the presence of cockle shell-derived CaCO_3 aragonite nanoparticles, natural polymers, and crosslinked and natural copolymer in the scaffolds. Kamba and Zakaria⁴⁰ earlier described the cockle shell-derived calcium carbonate nanocrystal as a potent facilitator of osteoblast proliferation, differentiation, and adhesion. Tran and Webster⁴¹ observed proliferation and viability of cell deprived of obvious toxicity from a comparable research on pearl shell nanograde powder. HA-coated magnetic nanoparticles was also witnessed to cause improvement in the proliferation of osteoblast as compared to the uncoated form after 5 days of treatment.⁴² These observations revealed that osteoconduction, osteogenesis, and osteoinduction ensue concurrently in the animals implanted with non-seeded 5211_{GTA+Alginate} scaffolds, whereas in animals

implanted with non-seeded 5211 and 5211_{PLA} scaffolds, only osteoconduction was seen, and hence formation of new bone was slow and incomplete. Our result is in agreement with those of Li and Li⁴³ and Schnettler et al.⁴⁴

Previous research on the formation of new bone on scaffolds after implantation using diverse types of scaffolds has revealed diverse period of formation of new bone. Martin et al⁴⁵ in their study positioned a block of HA in the cortical humerus defects and radius in dogs; the results showed that the interposition of bone in pores began from 52% at week 16 to 74% at 12 months (quantity of bone in relation to the pore space) post-implantation. The spongy bone regrowth was 38% after 4 weeks and raised to another 17% at 1 year; nonetheless the pore spaces of HA hardly entirely occupied the bone throughout that time.⁴⁶ Vuola et al⁴⁷ used the coral implant and reported that after 6 weeks of implantation, the bone could not really occupy the pores of coral sample; nevertheless it substituted the matrix. Yoshikawa et al⁴⁸ established that HA-improved implants required a high quantity of new cells from bone marrow and that the technique would be challenging in clinical application. Additionally, the bone-forming ability of these transplants is yet to be resolved after termination of immunosuppressive agents. Chitosan surface-modified poly (D, L-lactic acid) scaffolds investigation was carried out by Cai et al⁴⁹ after implantation for 12 weeks. Many new bones were fashioned in the scaffolds at that time point with a minor inflammatory response. This concept is in conflict with the discovery that no foreign body (macrophages) responses are noticed around the implants.⁵⁰ A minute new bone linked to the scaffolds starts forming circles around the scaffolding, which is yet to be totally absorbed. The earlier results revealed significantly different time periods for the defects to be completely healed compared to the current results. The H&E and Masson's trichrome stained sections clearly showed the healing of the defect sites. All defects healed from the margins to the center with most healing noted at the margins in animals implanted with 5211 and 5211_{PLA} scaffolds, and from center to the margins in animals implanted with 5211_{GTA+Alginate} scaffold. These findings were further confirmed by radiographic analysis. The nanocomposite scaffold-implanted defect showed the most systematic healing, which clearly indicated a guided tissue formation.

According to Rath et al, it is vital for a porous scaffold to facilitate the migration of cells to the center cavity in order to be classified as functionally useful.⁵¹ Underlying these cells are networks of collagen-like connective tissues that are found around the periphery of newly deposited osteoid

tissues that are further surrounded by mineralizing bone tissues with presence of blood vessels and osteocytes containing lacunae. These findings show that the scaffold 5211_{GTA+Alginate} has sufficient porosity and morphological structural properties that allow penetration of bone cells as well the ability to support sufficient vascularization in order to support bone healing and remodeling processes. The deposition of collagen indicates the partial osteoinductive property of a scaffold that has potential biomimetic features as reported in a study by Liuyun et al⁵² on nano-HA/chitosan/carboxymethyl cellulose composite scaffolds.

The presence of blood vessels in the newly formed tissues is another indicator of efficient angiogenic response of the native tissue toward the implanted scaffold materials. The presence of sufficient vascularization and transport system ensures adequate supply and exchange of nutrients and wastes that is crucial in supporting cell survival and growth for a longer period as well as for construction of larger amount of tissues.⁵³ Findings on the active infiltration of osteoblast cells and the neo-vascularization properties of the scaffolds allow further justifications on the excellent osteoconductive nature of the developed nanocomposite scaffold. Ghanaati et al⁵⁴ in their study emphasized that osteoblasts cells act as an inbuilt biological signal that promotes the neo-vascularization process from the host tissues and that the ability of these cells to actively populate the scaffold structure further enhances the healing properties.

One important finding from the histological examination is regarding the quality of the regenerated tissues. The nanocomposite scaffold-implanted defect showed a more homogenous form of tissue formation throughout the entire defect compared to the empty defect, which showed signs of healing with minimal formation of regenerated tissue with a higher amount of connective tissues on the upper surface section with underlying distorted tissue and marrow components. A study by González-Toro and Thayumanavan³⁰ and Díaz-Rodríguez et al³¹ previously reported findings in which bone marrow tissues were found to evolve to fill in the spaces left empty following complete resorption of a scaffold material. In regards to this, the healing of the empty defect sites are facilitated with the use of a scaffold, thus causing the defect sites to be filled with the underlying bone marrow tissues with scarcely forming bone tissues interspersed in a majority of these defect sites. These histological findings possibly explain the gross appearance of the bone tissue specimen of the empty defect site that was found to be present with an almost uncompleted closure of the defect site at the time of retrieval.

The healing of the control group, on the other hand, was found to be highly based on connective tissue; in the control group a slower rate and minimal extent of bone maturation, as observed in the Masson's trichrome stained images, was found compared to the nanocomposite scaffolds groups in which a greater extent of bone maturation was found. The cockle shell-derived CaCO_3 aragonite nanoparticles powder potentially acted as an external source of calcium that enhanced the formation of bone tissues in the nanocomposite scaffolds. It has been previously speculated that an increase in extracellular calcium concentration from an external source possibly acts to downregulate the osteoclastic activity, without disturbing osteoblastic differentiation, leading to a favorable amount of total bone tissue formation.⁵⁵ This probably explains the higher amount of bone tissues found within the nanocomposite scaffolds groups as initial degrading of the scaffold materials would have observed an influx in the external source of calcium concentration that could have promoted higher osteoblastic activity at an earlier stage. This early stage bone formation possibly explains the presence of higher amount of mineralized bone tissues within the nanocomposite defect site that is indicative of a faster healing property.

In additionally, lacunae containing osteocytes as well as osteoclasts cells were observed in the surfaces newly formed bone tissues in the nanocomposite scaffold implanted site, which was indicative of active regeneration and remodeling activity. The presence of both osteoblast and osteoclast cells is an important finding that shows the mechanism of bone formation and resorption, as well as the subsequent remodeling process at work. The entire process is likely promoted by the degradation of the scaffolds that release nano-cockle shell powder that has potentials in accelerating bone formation as proven previously by *in vitro* evaluations (unpublished data). Comparable findings were also reported by Jin et al³⁹ in a work carried out on the active generation of bone tissues due to the degradation of HA from the HA/chitosan-alginate composite scaffolds.

An important criterion often highlighted in the field of scaffold fabrication for the purpose of tissue engineering is the biodegradability or bioresorbability of a scaffold material, given the primary aim of the scaffold is to serve as a temporary support.⁵⁶ In regards to this, histological observations pointed to a well-degraded scaffold material. The degrading pattern of the nanocomposite scaffold was found to be directly proportional to the formation of the new bone tissues. This early loss of structure may have contributed to the structural collapse of the scaffolds porous networks leading to a poorer quality of healing observed at the mid and margin sections of the defect site. The slower degradation

rate of the nanocomposite scaffolds, on the other hand, proves to be an added advantage as it provides sufficient structural support for the newly generating bone tissues, given the fact that bioresorbability is an important factor that determines bone tissue regeneration. The ideal scaffold material should show degrading properties parallel to the regeneration of new tissues in an appropriate rate to support the new tissue formation.⁵⁷ It is also crucial for the scaffold material to degrade in a timely manner to allow the formation of sufficient extracellular matrices to occupy void places occurring at sites where the scaffolds have degraded.^{56,58} With the use of the nanocomposite scaffolds, the amount of void areas evaluated were also found to be lesser compared to the empty defect, thereby further justifying the superiority of the nanocomposite scaffold.

Regarding the degrading behavior of the scaffold materials, no adverse tissue reactions were observed within the defect site. Histopathologically, there were no evidences of chronic inflammatory reactions at the end point of the experimental time frame. Small amounts of infiltrates, however, could be observed toward the center cavity integrated together with high numbers of osteoblast cells. This, however, points to a favorable scenario, in which the degrading scaffold material acts as an attraction force toward the recruitment of inflammatory cells that were microscopically evident in the center cavity of the defects in the scaffold implanted site but not within the empty defects. According to Ghanaati et al,⁵⁴ this attraction force exerted by the degrading biomaterials has potential benefits in facilitating the process of angiogenesis due to the fact that these inflammatory cells are capable of producing vascularization-promoting proteins. This increased vascularization process is what underlies the improved bone tissue formation and healing rate observed within the scaffold implanted defect sites compared to the empty defects with higher intensity noted within the nanocomposite implanted site. The presence of these minute amounts of inflammatory infiltrates and well-formed bone tissues and osteoids along the periphery of the defect margins also shows the lack of toxicity of the implanted scaffold toward the host tissues and a well-integrated scaffold host interface.

Any signs of inflammation speculated at the early stage of healing as a normal tissue reaction toward a foreign object is shown to be not persisting by week 8 post-implantation of the study. Comparatively, the study by González-Toro and Thayumanavan³⁰ and Díaz-Rodríguez et al³¹ on bioactive injectable cements in varying formulation on a similar kind of animal model reported on the presence of inflammatory cells still remaining localized around the defect sites after 24 weeks of the study duration. The absence of excessive

inflammatory response by the host tissue toward the degrading scaffold material in this study gives further justification toward the histocompatibility of the developed scaffolds.

Conclusion

Our results revealed that the cockle shell-derived CaCO₃ aragonite nanocomposite 3D scaffolds performed excellently in restoring the segment defect in long-term assessment trials. It is noteworthy to mention that there was no toxic or any adverse reactions noticed in all the pre-fabricated materials implanted into the animal model. The cockle shell-derived CaCO₃ aragonite nanocomposite 3D scaffolds demonstrated superior qualities in controlling complete growth of new bone alongside the segmental bone defect when assessed by histological study.

Acknowledgments

The authors thank the Faculty of Veterinary Medicine, Universiti Putra Malaysia, for supporting this study. This research was supported by Malaysian Government under Science fund number 02-01-04-SF1378.

Author contributions

All authors contributed toward data analysis, drafting and revising the paper and agree to be accountable for all aspects of the work.

Disclosure

The authors report no conflicts of interest in this work.

References

1. Bobynd JD, Stackpool GJ, Hacking SA, Tanzer M, Krygier JJ. Characteristics of bone ingrowth and interface mechanics of a new porous tantalum biomaterial. *J Bone Joint Surg.* 1999;81B(5):907–914.
2. Shin DS, Choong PF, Chao EY, Sim FH. Large tumor endoprostheses and extracortical bone-bridging: 28 patients followed 10–20 years. *Acta Orthop Scand.* 2000;71(3):305–311.
3. Tanzer M, Turcotte R, Harvey E, Bobynd JD. Extracortical bone bridging in tumor endoprostheses. Radiographic and histologic analysis. *J Bone Joint Surg.* 2003;85A(12):2365–2370.
4. Aho AJ, Eskola J, Ekfors T, Manner I, Kouri T, Hollmen T. Immune responses and clinical outcome of massive human osteoarticular allografts. *Clin Orthop Relat Res.* 1998;346(346):196–206.
5. Zimmermann G, Moghaddam A. Allograft bone matrix versus synthetic bone graft substitutes. *Injury.* 2011;42(Suppl 2):S16–S21.
6. Lindahl H, Malchau H, Herberts P, Garellick G. Periprosthetic femoral fractures classification and demographics of 1049 periprosthetic femoral fractures from the Swedish national hip arthroplasty register. *J Arthroplasty.* 2005;20(7):857–865.
7. Hacking SA, Harvey EJ, Tanzer M, Krygier JJ, Bobynd JD. Acid-etched microtexture for enhancement of bone growth into porous-coated implants. *J Bone Joint Surg.* 2003;85B(8):1182–1189.
8. Hallan G, Lie SA, Furnes O, Engesaeter LB, Vollset SE, Havelin LI. Medium and long-term performance of 11,516 uncemented primary femoral stems from the Norwegian arthroplasty register. *J Bone Joint Surg.* 2007;89B(12):1574–1580.

9. Lind M, Bunker C. Factors stimulating bone formation. *Eur Spine J.* 2001;10:S102–S109.
10. Gasser B. About composite materials and their use in bone surgery. *Injury.* 2000;31(Suppl 4):48–53.
11. Sawyer-Glover AM, Shellock FG. Pre-MRI procedure screening: recommendations and safety considerations for biomedical implants and devices. *J Magn Reson Imaging.* 2000;12(1):92–106.
12. Shellock FG. Biomedical implants and devices: assessment of magnetic field interactions with a 3.0-tesla MR system. *J Magn Reson Imaging.* 2002;16(6):721–732.
13. Geiger M, Li RH, Friess W. Collagen sponges for bone regeneration with rhBMP-2. *Adv Drug Deliv Rev.* 2003;55:1613–1629.
14. Young S, Wong M, Tabata Y, Mikos AG. Gelatin as a delivery vehicle for the controlled release of bioactive molecules. *J Control Release.* 2005;109:256–274.
15. Azami M, Mohammad R, Fathollah M. Gelatin/hydroxyapatite nanocomposite scaffolds for bone repair. *Soc Plastic Eng.* 2010:1–3.
16. Nandi SK, Mukherjee RP, Kundu B, De DK, Basu D. Orthopaedic applications of bone graft and graft substitutes: a review. *Indian J Med Res.* 2010;132:15–30.
17. Lee K, Silva E, Mooney D. Growth factor delivery-based tissue engineering: general approaches and a review of recent developments. *J R Soc Interface.* 2011;8(55):153–170.
18. Johnson AL, Stein LE, Roe SC. Evaluation of collagen as a retainer for autogenous cancellous bone used in repair of full thickness cortical bone defects. *Vet Surg.* 1987;16(2):146–150.
19. Zuki AB, Bahaa FH, Noordin MM. Cockle shell-based biocomposite scaffold for bone tissue engineering. *Reg Med Tis Eng Cells Biomater.* 2011:365–390.
20. Bharatham H, Zuki ABZ, Perimal EK, Loqman MY, Hamid M. Development and characterization of novel porous 3D alginate-cockle shell powder nanobiocomposite bone scaffold. *BioMed Res Int.* 2014;2014(146723):1–12.
21. Jorge-Herrero E, Fernandez P, Turnay J, et al. Influence of different chemical cross-linking treatments on the properties of bovine pericardium and collagen. *Biomaterials.* 1999;20:539–545.
22. Kim HM, Miyaji F, Kokubo T, Nishiguchi S, Nakamura T. Graded surface structure of bioactive titanium metal prepared by chemical treatment. *J Biomed Mater Res.* 1999;45:100–107.
23. Lee S, Kim SH, Han Y, Kim Y. Synthesis and degradation of end-group functionalized polylactide. *J Polym Sci A Polym Chem.* 2001;39:973.
24. Chen JH, Liu QL, Zhang XH, Zhang QG. Pervaporation and characterization of chitosan membranes cross-linked by 3-aminopropyltriethoxysilane. *J Membr Sci.* 2007;292:125–132.
25. Bucholz RW, Carlton A, Holmes R. Interporous hydroxyapatite as a bone graft substitute in tibial plateau fractures. *Clin J Orthop.* 1989;240:53–62.
26. Krajewski A, Ravaglioli A, Roncari E, Pisco P, Montanari L. Porous ceramic bodies for drug delivery. *J Mater Sci Mater Med.* 2000;11:763–772.
27. Zeltinger J, Sherwood JK, Graham DA, Mueller R, Griffith LG. Effect of pore size and void fraction on cellular adhesion, proliferation and matrix deposition. *Tis Eng.* 2001;7:557–572.
28. Kim HW, Knowles JC, Kim HE. Development of hydroxyapatite bone scaffold for controlled drug release via poly (epsilon-caprolactone) and hydroxyapatite hybrid coatings. *J Biomed Mater Res.* 2004;70B:240–249.
29. Gonzalez C, Mariam AS, Manuela DLT, et al. Injectable and self-curing composites of acrylic/bioactive glass and drug systems. A histomorphometric analysis of the behavior in rabbits. *Biomaterials.* 2006;27(9):1778–1787.
30. González-Toro DC, Thayumanavan S. Advances in polymer and polymeric nanostructures for protein conjugation. *Eur Polym J.* 2013;49:2906–2918.
31. Diaz-Rodríguez P, González P, Serra J, Landin M. Key parameters in blood-surface interactions of 3D bioinspired ceramic materials. *Mater Sci Eng C.* 2014;41:232–239.

32. Mahmood SK, Zakaria MZAB, Razak ISBA, et al. Preparation and characterization of cockle shell aragonite nanocomposite porous 3D scaffolds for bone repair. *Biochem Biophys Rep.* 2017;10:237–251.
33. Enlow DH, Brown SO. A comparative histological study of fossil and recent bone tissues. Part III. *Texas J Sci.* 1958;10:187–230.
34. Donath K, Rohrer MD, Beck-Mannagetta J. A histologic evaluation of a mandibular cross section one year after augmentation with hydroxyapatite particles. *Oral Surg Oral Med Oral Pathol.* 1987;63(6):651–655.
35. Badar M, Lünsdorf H, Evertz F, et al. The formation of an organic coat and the release of corrosion microparticles from metallic magnesium implants. *Acta Biomater.* 2013;9:7580–7589.
36. Thompson RC, Garg JA, Clohisy DR, Cheng EY. Fractures in large segment allografts. *Clin Orthop Relat Res.* 2000;370:227–235.
37. Nishida J, Shimamura T. Methods of reconstruction for bone defect after tumor excision: a review of alternatives. *Med Sci Monitor.* 2008;14(8):RA107–RA113.
38. Okada Y, Suka T, Sim FH, Gorski JP, Chao EY. Comparison of replacement prostheses for segmental defects of bone. Different porous coatings for extracortical fixation. *J Bone Joint Surg.* 1988;70A(2):160–172.
39. Jin HH, Kim DH, Kim TW, et al. In-vivo evaluation of porous hydroxyapatite/chitosan-alginate composite scaffolds for bone tissue engineering. *Int J Bio Macromol.* 2012;51(5):1079–1085.
40. Kamba SA, Zakaria ZAB. Osteoblasts growth behavior on bio-based calcium carbonate aragonite nanocrystal. *BioMed Res Int.* 2014;2014:(215097).
41. Tran N, Webster TJ. Increased osteoblast functions in the presence of hydroxyapatite-coated iron oxide nanoparticles. *Acta Biomater.* 2011;7(3):1298–1306.
42. Choi S-J, Oh J-M, Choy J-H. Toxicological effects of inorganic nanoparticles on human lung cancer A549 cells. *J Inorg Biochem.* 2009;103(3):463–471.
43. Li Z, Li ZB. Repair of mandible defect with tissue engineering bone in rabbits. *ANZ J Surg.* 2005;75:1017–1021.
44. Schnettler R, Pfefferle H-J, Kilian O, et al. Glycerol-1-lactide coating polymer leads to delay in bone ingrowth in hydroxyapatite implants. *J Control Release.* 2005;106(1–2):154–161.
45. Martin RB, Chapman MW, Sharkey NA, Zissimos SL, Bay B, Shors EC. Bone ingrowth and mechanical properties of coralline hydroxyapatite 1 year after implantation. *Biomaterials.* 1993;14(5):341–348.
46. Rosen HM, McFarland MM. The biologic behavior of hydroxyapatite implanted into the maxillofacial skeleton. *Plastic Reconstr Surg.* 1990;85(5):718–723.
47. Vuola J, Göransson H, Böhling T, Seljavaara A. Bone marrows induce osteogenesis in hydroxyapatite and calcium carbonate implants. *J Biomater.* 1995;17:1761–1766.
48. Yoshikawa T, Nakajima H, Yamada E, et al. In vivo osteogenic capability of cultured allogeneic bone in porous hydroxyapatite: immunosuppressive and osteogenic potential of FK506 in vivo. *J Bone Miner Res.* 2000;15:1147–1157.
49. Cai K, Yao K, Yang Z, Qu Y, Li X. Histological study of surface modified three dimensional poly (D, L-lactic acid) scaffolds with chitosan in vivo. *J Mater Sci Mater Med.* 2007;18:2017–2024.
50. Hautamäki M. *Repair of Segmental Bone Defects with Fiber-Reinforced Composite: A Study of Material Development and an Animal Model on Rabbits* [PhD thesis]. Turku, Finland: Annales Universitatis Turkuensis; 2012.
51. Rath SN, Strobel LA, Arkudas A, et al. Osteoinduction and survival of osteoblasts and bone marrow stromal cells in 3D biphasic calcium phosphate scaffolds under static and dynamic culture conditions. *J Cell Mol Med.* 2012;16(10):2350–2361.
52. Liyun J, Yubao L, Chengdong X. Preparation and biological properties of a novel composite scaffold of nano-hydroxyapatite/chitosan/carboxymethyl cellulose for bone tissue engineering. *J Biomed Sci.* 2009;16(1):65.
53. Li Z, Ramay HR, Hauch KD, Xia D, Zhang M. Chitosan–alginate hybrid scaffolds for bone tissue engineering. *Biomaterials.* 2005;26:3919–3928.
54. Ghanaati S, Unger RE, Webber MJ, et al. Scaffold vascularization in vivo driven by primary human osteoblasts in concert with host inflammatory cells. *Biomaterials.* 2011;32(32):8150–8160.
55. Pabbruwe MB, Standard OC, Sorrell CC, Howlett CR. Bone formation within alumina tubes: effect of calcium, manganese and chromium dopants. *Biomaterials.* 2004;25(20):4901–4910.
56. Cheung H, Lau K, Lu T, Hui D. A critical review on polymer-based bio-engineered materials for scaffold development. *Compos B Eng.* 2007;38(3):291–300.
57. Bose S, Roy M, Bandyopadhyay A. Recent advances in bone tissue engineering scaffolds. *Trends Biotechnol.* 2012;30(10):546–554.
58. Wen-De X, Zhao-Ming Z, Yong-Zhi T, Zi-Xing X, Zhun X, Jian-Ting C. Repair of critical size bone defects with porous poly (D, L-lactide)/nacre nanocomposite hollow scaffold. *Saudi Med J.* 2012;33(6):601–607.

International Journal of Nanomedicine

Publish your work in this journal

The International Journal of Nanomedicine is an international, peer-reviewed journal focusing on the application of nanotechnology in diagnostics, therapeutics, and drug delivery systems throughout the biomedical field. This journal is indexed on PubMed Central, MedLine, CAS, SciSearch®, Current Contents®/Clinical Medicine,

Submit your manuscript here: <http://www.dovepress.com/international-journal-of-nanomedicine-journal>

Dovepress

Journal Citation Reports/Science Edition, EMBase, Scopus and the Elsevier Bibliographic databases. The manuscript management system is completely online and includes a very quick and fair peer-review system, which is all easy to use. Visit <http://www.dovepress.com/testimonials.php> to read real quotes from published authors.